








Optical Real-Time Castability Evaluation for High-Throughput Glass Melting

S. Gogula¹, H. Bornhöft¹, L. Wondraczek², M. Sierka²,
A. Diegeler³, R. Müller^{1,4,*}, J. Deubener¹

¹ Clausthal University of Technology, Germany

² Friedrich-Schiller-Universität Jena, Germany

³ Fraunhofer Institute for Silicate Research ISC, Germany

⁴ Bundesanstalt für Materialforschung und -prüfung (BAM), Germany

*Correspondence: Ralf Müller, ralf.mueller@tu-clausthal.de

Abstract. A novel optical real-time method for evaluating the castability of glass forming melts for laboratory furnaces is presented. The method is based on the analysis of top view images of the melt surface inside the crucible during melting after being subjected to a small mechanical impulse. In this way, the melt surface is excited to oscillate. The difference in contrast between two images taken in quick succession scales with the viscosity, with a larger difference occurring at lower viscosities. The method is designed as an instrument for the in-line evaluation of the castability for a high-throughput glass melting system as part of the joint project “GlasDigital” in the framework of the German Platform Material Digital initiative but is applicable to other laboratory furnaces as well.

Keywords: Optical Real-Time Castability Check, High-Throughput Melting, Image Analysis

1. Introduction

The largely infinite adjustability of their chemical composition and unique shaping techniques make glasses promising customised materials for future technologies. Their almost unlimited variety [1], their wide range of applications [2], [3], and their challenging target property profiles, however, place ever increasing demands on glass development. In the framework of the German “Plattform MaterialDigital” of the Federal Ministry of Education and Research (BMBF), the joint project “GlasDigital” was therefore focused on novel high-throughput (HT) concepts that embed HT robotic glass melting systems, HT glass analysis tools, glass databases, and machine learning tools for data mining, property and process prediction in to an ontology-based digital infrastructure [4].

HT robotic glass melting systems, however, are still at an early stage of development. To use their full system capacity, they must be able to deal with various possible process failures. Among others, such as incomplete batch melting, foaming over, or incorrect cooling, the evaluation of the castability of the melt is highly important.

This article presents a novel optical real-time method for evaluating the castability of the melt. For this purpose, the melt inside the furnace is monitored with a camera after being subjected to an external mechanical impulse that causes small vibrations of the melt surface. Depending on viscosity, these vibrations vary in intensity and are limited in time. In this way,

castability can be derived from real-time analyses of successive images. The speed and simplicity of the method is based on the continuous camera observation of the melt inside the furnace and the minimised effort required for image processing.

2. Experimental setup

The method was demonstrated for the electric chamber furnace LHT 01/17 LB speed (Nabertherm GmbH, Lilienthal, Germany), which is equipped with lifting floors for fast robotic crucible loading (Figure 1) and loaded with a cylindrical Pt/Rh crucible ($h = 70$ mm, $\varnothing = 60$ mm).

A digital camera (VCXG-15C.I, Baumer GmbH, Friedberg, Germany) was used to monitor the glass melt inside the furnace. Its global shutter allows exposure times between 0.001 and 60000 ms. The camera is equipped with a Sony IMX273 Gen2 1/2.9" CMOS chip, which provides 8-bit 1440×1080 pixels colour images.

The camera was mounted on top of the furnace to observe the melt (Figure 1 top left). The C-mounted 35 mm Ricoh lens with small aperture allowed a representative view onto the melt surface through a narrow corundum tube (10 mm inside diameter, 130 mm length) built into the furnace roof. A continuous intake airflow prevents the condensation of volatile melt components on the tube wall.

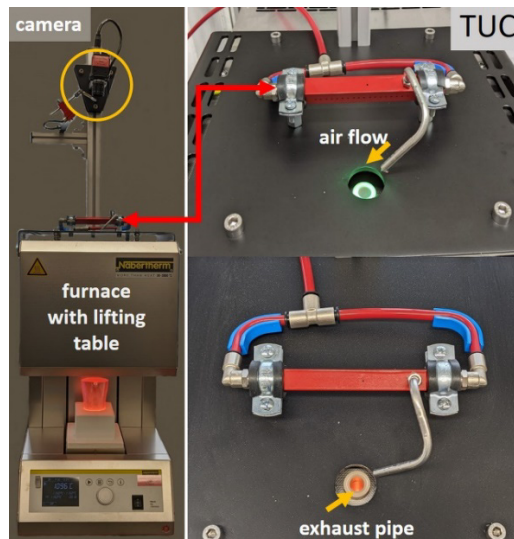


Figure 1. Experimental setup of furnace, monitoring camera and image acquisition.

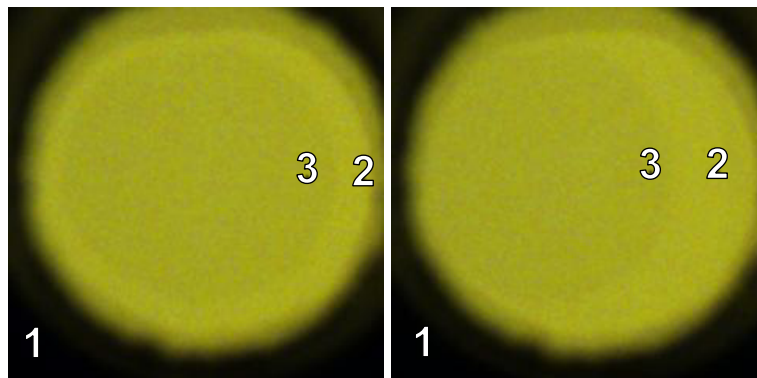


Figure 2. Top view images of the glass melt surface shortly after applying a mechanical pulse on the melting furnace. The second image (right) was taken $\Delta t = 30^{-1}$ s after the first one (left). (1) is the corundum tube with an opening of 10 mm diameter. The slightly darker area inside (3) is the reflected image of the cold observation tube in the hot furnace roof (2).

Figure 2 left shows the accessible top view onto the crucible covering 240x240 pixels. The outer dark region (1) reflects the corundum tube wall and its 10 mm opening. The inner circular light grey area (3) reflects the cold tube opening, contrasted by the surrounding brighter hot furnace roof (2). The Pt/Rh-crucible wall is not seen in this image section.

3. Image data acquisition

After waiting for a constant furnace temperature, image data acquisition at 30 fps was started for 60 s. During this time, small mechanical impacts ("pings") were manually applied on the furnace table to cause oscillations of the melt surface inside the crucible. The camera software (Baumer Camera Explorer, Windows version v3.4.2 for 64-bit Microsoft Windows 10) was then used to capture and store data via the supplied Gigabit Ethernet connection. Figure 2 shows two consecutive jpg images taken immediately after such a mechanical impulse, where local grey scale differences are evident. In the right image, which was taken $\Delta t = 30^{-1}$ s after the left one, the reflected tube opening appears displaced to the left and reveals a slightly inclined melt surface.

4. Image analysis

The consecutive images were processed using a Python script implementing widely known image processing routines [5], [6], provided by the open-source standard image processing library OpenCV [7]. Although the method is demonstrated here on stored jpg images, it was designed as an effective and reliable tool for real-time process control. The image analysing steps explained below were therefore designed to optimise sensitivity and calculation effort.

Step 1 converts the 240x240 pixel 8-bit colour camera images, $RGB(x,y)_t$, into 8-bit grey-scale images, $I(x,y)_t$ according to Equation (1) where the weighing factors $c_R = 0.299$, $c_G = 0.587$, and $c_B = 0.114$ reflect the colour sensitivity of the human eye [8], and ensure normalization ($I, R, G, B = 0-255$). This step was implemented with the *OpenCV* function "grey = cv2.cvtColor(image, cv2.COLOR_BGR2GRAY)" and aims to correct the strongly varying brightness and colour conditions that occur with different glass compositions and melting temperatures.

$$I(x, y)_t = c_R R(x, y)_t + c_G G(x, y)_t + c_B B(x, y)_t \quad (1)$$

Step 2 improves the overall contrast of the images by applying a grey value histogram equalisation. The processed image, $I_{eq}(x,y)_t$ has a rectified cumulative grey value distribution $CDF_{eq}(I_{xy})_t$, which is calculated from the original cumulative grey value distribution $CDF(I_{xy})_t$, according to Equation (2) where the brackets indicate the rounding to retain integers, and Min_t and Max_t denote the minimum and maximum grey integer values of $I(x,y)_t$, respectively. The corresponding *OpenCV* function is "equalized = cv2.equalizeHist(grey)" [9], [10].

$$CDF_{eq}(I_{xy})_t = \left[\left(CDF(I_{xy})_t - Min_t \right) \cdot \frac{255}{Max_t - Min_t} \right] \quad (2)$$

Step 3 slices the images into quadrants of 120x120 pixels. The upper left and right quadrant packets in Figure 3 show the corrected grey value images $I_{eq}(x,y)$ and $I_{eq}(x,y)_{\Delta t}$, which were derived by step 1 and 2 from Figure 2 left and right, respectively. It can be seen that the image contrast is significantly increased. Step 3 would offer further possibilities of checking data consistency. For example, it seems unlikely that image changes caused by the displacement of the reflected image of the corundum tube due to inclinations of the melt surface only occur in one quadrant. Furthermore, since the inner rim of the reflected tube opening can be shifted out of two image quadrants while being shifted inwards in the other quadrants, systematically different grey value differences in these quadrants are to be expected. In the present analysis,

however, such features have not been implemented in order to ensure the shortest possible calculation times.

Step 4 reads out the absolute grey value difference between $\Delta I_{eq}(x,y)_t$ and $\Delta I_{eq}(x,y)_{t+\Delta t}$ for each quadrant (*OpenCV* function “diff = cv2.absdiff(quarter1, quarter2)” [7]:

$$\Delta I_{eq}(x,y)_t = |I_{eq}(x,y)_t - I_{eq}(x,y)_{t+\Delta t}| \quad (3)$$

The four thus calculated $\Delta I_{eq}(x,y)_t$ images (quadrants are not explicitly indexed for better readability) are shown in the lower left quadrant packet in *Figure 3*. These absolute differences, however, still did not prove to be sufficiently significant.

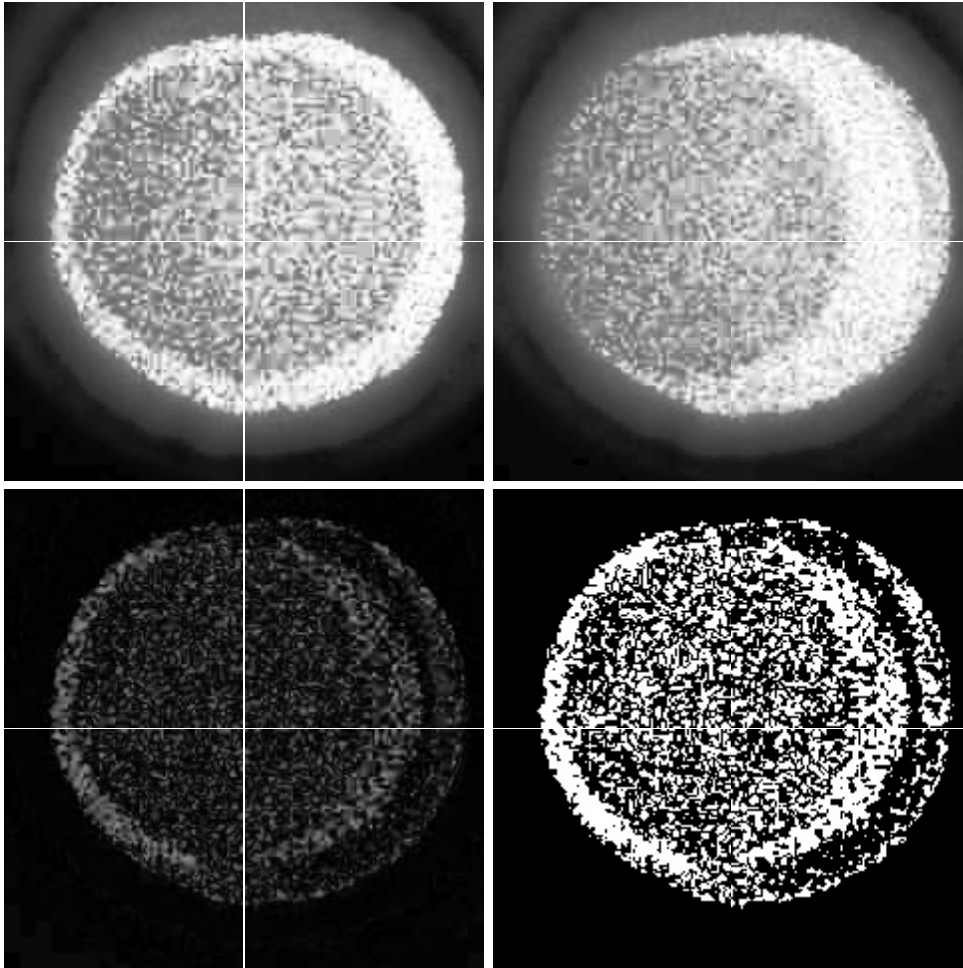


Figure 3. The packets on the left and right upper quadrant show the four corrected 8-bit grey value images, $I_{eq}(x,y)_t$ and $I_{eq}(x,y)_{t+\Delta t}$, for each quadrant which were derived from *Figure 2* left and right via step 1 - 3. The lower left quadrant packet shows the four 8-bit absolute grey value difference images, $\Delta I_{eq}(x,y)_t$, which were returned in step 4. The packet in the lower right quadrant shows the 2-bit image $\Delta I_{bw}(x,y)_t$ resulting from the threshold contrast enhancement in step 5.

Step 5 therefore applies a grey value threshold for further contrast enhancement. All $\Delta I_{eq}(x,y)_t \leq 30$ were set to zero (black = no change), while $\Delta I_{eq}(x,y)_t > 30$ was set to 255 (white = change) (*OpenCV* Python code “thresholded = cv2.threshold(cv2.cvtColor(diff, cv2.COLOR_BGR2GRAY), threshold_value, 255, cv2.THRESH_BINARY)”). A threshold limit of 30 proved to be most suitable. This could reflect the weak grey level value difference between the shifted light grey reflection of the tube opening in the hot furnace roof. Step 5 thus provides high-contrast binary images, $\Delta I_{bw}(x,y)_t$, shown in the lower right quadrant packet of *Figure 3*.

Step 6 provides a single quantity, D_t , measuring the image differences between the two consecutive images $I_{eq}(x,y)_t$ and $I_{eq}(x,y)_{t+\Delta t}$, by counting all white pixels in each quadrant (Open CV Python code "difference_pixel_count = np.sum(thresholded == 255)"). For a 120x120 pixels image, D_t varies between 0 and 14.400 and reflects the rate of image change for a given Δt .

5. Castability evaluation

To utilise the thus calculated D_t data for the evaluation of casting viscosity, the above procedure was applied to a reference glass at different temperatures. In this study, a sodium-alumino-borosilicate glass (34Na₂O-17Al₂O₃-17B₂O₃-32SiO₂ mol%) was used. The temperature ranged from 850 to 1250 °C. To ensure homogeneity, the fully melted and fined glass melt was cooled down from 1250 °C to 850 °C in the furnace before starting the experiment.

After ≈ 30 min, the temperature profile was well equalized, the continuous image data acquisition at 30 fps was started, and a series of manual impulses at regular intervals was applied. Data acquisition was then stopped, and the furnace was heated up to the next temperature, which again was hold for 30 min before data acquisition was started for 60 s. This procedure was repeated in 50 to 100 K steps until 1250°C was reached again.

Figure 4 shows $D(t)$ for different temperatures and the four quadrants Q1-Q4 comprising more than 1200 images (40 s acquisition time). The image acquisition time is represented in terms of image numbers. The mechanical impulses can be seen around image numbers 100, 400, 800 and 1200. These numbers correspond to $t \approx 3, 13, 26,$ and 40 s for the applied acquisition rate of 30 fps. At 950 - 1250 °C, significant peaks reflecting these mechanical impulses can be clearly detected from the noise level.

This background noise level ranges between 1500 at low temperature and 3500 at high temperature. It probably reflects various contributions such as noise from the camera sensor, air turbulences, surface vibrations due to mechanical vibrations in the environment, and furnace vibrations caused by the electrical heating system. All these contributions should increase with temperature, as actually seen in Figure 4. The different noise level in different quadrants could be related to the different position of the reflected rim of the cold tube opening in the furnace roof, as its displacement causes the strongest grey value differences.

However, to keep the castability evaluation as fast as possible, we avoided the time-consuming calculations of this noise level and the application of $D(t)$ peak analysis routines. Instead, we calculated the *coefficient of variation* of $D(t)$ for every 250 values of $D(t)$ according to:

$$CV_D(T) = \sigma \left(\frac{D(t,T)}{\langle D(t,T) \rangle} \right) \quad (4)$$

where $\langle D(t,T) \rangle$ is the mean value of this 250-image subseries measured at the temperature T and σ the standard deviation of $D(t,T)/\langle D(t,T) \rangle$. This way, a value of $CV_D(T)$ can be calculated every 8 s.

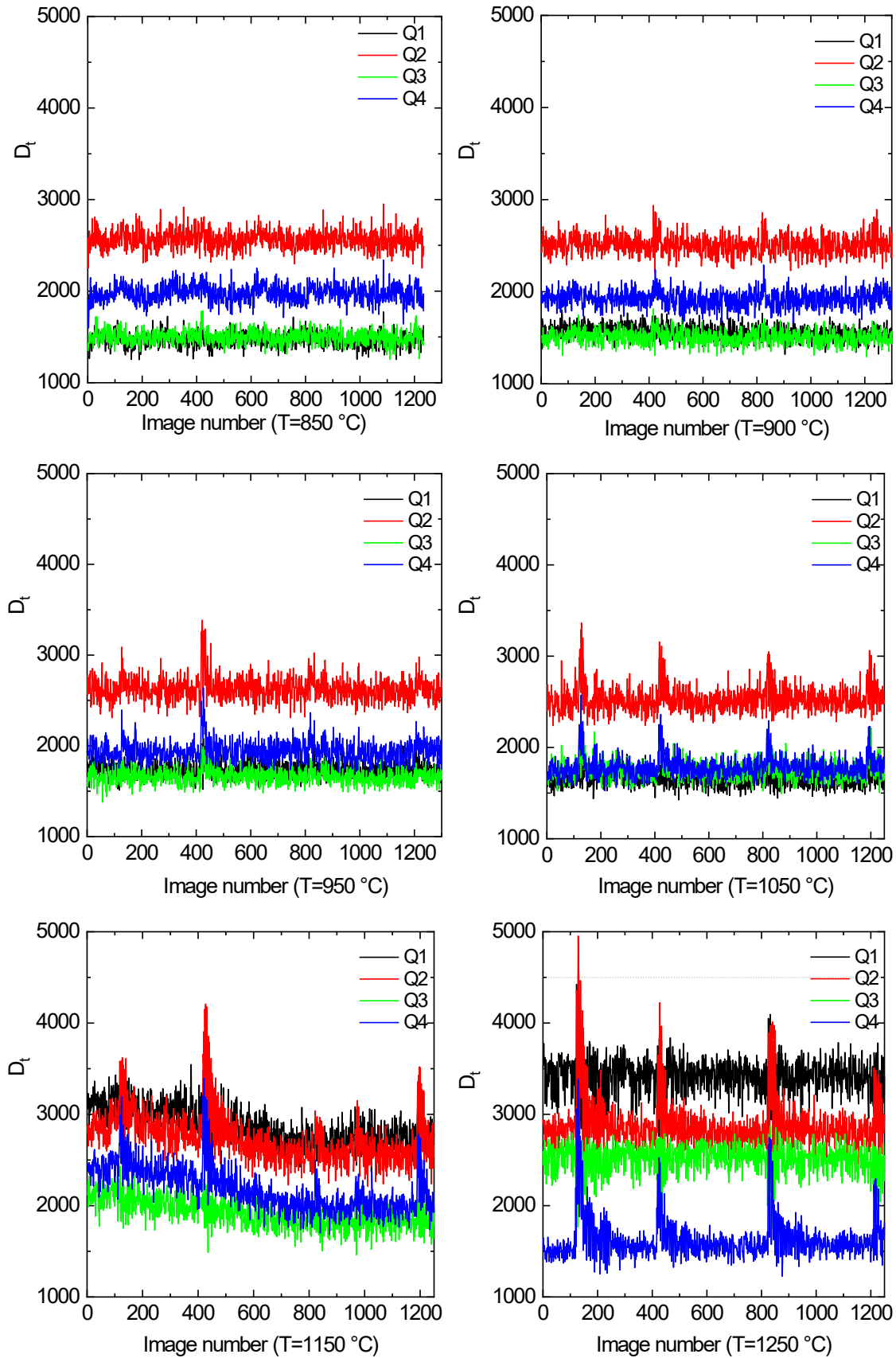


Figure 4. $D(t)$ for different temperatures, T . The image number 1200 corresponds to 40 s due to the applied image acquisition at 30 fps.

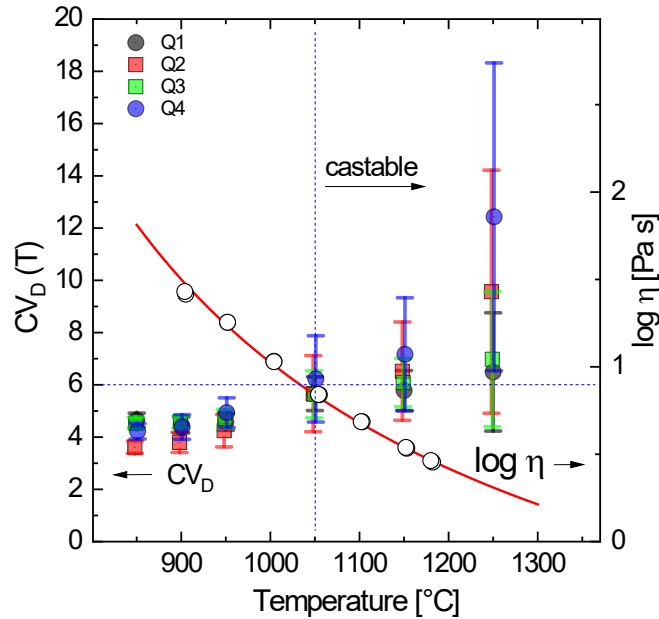


Figure 5. Calculated coefficient of variation, $CV_D(T)$, for the different quadrants (left ordinate) and viscosity data (right ordinate) for the glass under study as a function of temperature. The red curve is the VFT fit to all measured viscosity data including the isokom temperature T_{12} ($\log \eta/\text{Pa s} = 12.3$) = 484 °C with $A = -1,41$, $B = 1534^\circ\text{C}$, and $C = 372^\circ\text{C}$.

To correlate $CV_D(T)$ in Figure 5 with viscosity, η , it was measured with rotational viscometry (RV 20, Haake Mess-Technik GmbH u. Co., Karlsruhe, Germany) at temperatures > 900 °C. In addition, the isokom temperature, $T_{12} = 484$ °C, where $\log (\eta/\text{Pa s}) = 12.3$, was determined using optical dilatometry (DIL 806, TA Instruments, Eschborn, Germany). The results are included in Figure 5 (right ordinate, open circles). The curve is the VFT fit of all data (T_{12} is not shown in Figure 5). It is seen that $CV_D(T) > 6$ roughly correlates with $\eta < 10$ Pa s. This value intuitively indicates very good melt castability as the viscosity for water, olive oil, and honey at 20 °C are $\approx 10^{-3}$, 10^{-1} , and 10 Pa s, respectively [11]. At such low viscosity, a good homogenisation of the melt is also expected due to convective flow and an easy up rise of gas bubbles. In this sense, the proposed procedure can also give an indication of an appropriate fining temperature.

6. Discussion

(1) The method described above offers interesting advantages. First, as it is based on a continuous melt observation and the image analysis has been kept as simple as possible, it offers a real-time control of the castability of the melt. Nevertheless, Figure 5 proves its applicability between 950 and 1250 °C for the sodium-alumino-borosilicate glass under study, where good castability found in the experiments roughly correlates with $CV_D(T) > 6$ and $\eta < 10$ Pa s.

A second advantage is the simplicity of the method. Since the mechanical impulse that causes the surface vibration of the melt is generated during furnace operation, no additional process step associated with an interruption of melting is required. Apart from the monitoring camera and the observation tube, which can also be used for other purposes such as batch melting or foam control, no special technical equipment is required. This makes the method easy applicable to any laboratory furnace that allows melt observation from above. The uncertainties in time and intensity caused by the manual generation of the mechanical impulse are balanced out by averaging over several impulses regardless of their time sequence.

Further advantages could result from implementing the method in a HT glass melting system. In particular, $V_D(T)$ can be used here as an adjustable query system parameter that interrupts improperly programmed casting steps as an emergency stop. This feature would reduce

the probability of system failure. Furthermore, without automated reliable castability checks, the casting time must be programmed longer than actually required to provide extra safety margins. Such casting delay outside the furnace would exponentially increase viscosity with time due to rapid temperature radiation losses. With higher casting viscosity, however, various process failures become more likely such as drawing glass threads, misplacing, or even crashing the poured glass sample, sticking to the robot gripper or other system components. In this way, real-time castability checks increase the melting system capacity. As the method enables the detection of low viscosity, it also ensures better casting reproducibility and helps to reduce the amount of melt remaining in the crucible after casting. As a further advantage, the reliability and sensitivity of the method would benefit from being implemented in a HT glass melting system, since it would allow to process non-compressed camera data. Finally, automated mechanical impulse generation can be implemented into the melting system, which would make it more repeatable and tuneable.

(2) As part of this study, various alternate methods for estimating a real-time castability check were considered. For example, the flowability of the melt was tested by tilting the crucible outside the melting furnace. However, this method was discarded after few tests as the melt cooled very quickly and any correction of this effect would have required time-consuming irradiation–temperature–viscosity simulations and the knowledge of the thermal materials parameters. Moreover, there were large differences in brightness between the hot crucible and its cold surroundings. Even with IR-capable equipment, the optical detection of small melt inclinations by observing the shift of low-contrast reflections of a reference object (such as the cold tube opening inside the furnace) was not possible.

Rotational viscometry inside the melting furnace would have been another interesting alternate for a castability evaluation. For the configuration presented here, however, the optical path through the corundum tube would be blocked and could no longer be used for continuous melt monitoring. A separate opening in the furnace roof would reduce the homogeneity of the furnace temperature and the achievable temperature maximum. In addition, Pt-cylinders must be immersed into the melt without prior knowledge of the current viscosity. Last but not least, these Pt tools must be replaced and cleaned after each service. An alternative version of this concept would be the use of top-loading, e.g., induction-heated furnaces for the final melting step. This concept would have similar disadvantages, but would allow the use of Pt stirrers for simultaneous measurements of shear viscosity and homogenisation of the melt.

(3) As the proposed optical method is kept as simple as possible to allow real-time castability evaluations, it underlies several application limits. Even though CV_D , scales with viscosity, and although its minimum value found for good castability ($CV_D(T) > 6$) well correlates with a reasonable upper viscosity limit ($\eta < 10$ Pa s) for the glass under study, we strongly advise against using the method for a quantitative estimation of $\eta(T)$. The deflection of the melt surface level, measured by CV_D , does not entirely reflect $\eta(T)$. As it represents a forced liquid oscillation, it also depends on crucible geometry, melt density, surface tension and the frequency-amplitude distribution of the applied mechanical impulse. Although surface tension and density scale much less with temperature and composition than $\eta(T)$ [3], which thus decides whether or not liquid oscillations are detectable in a given time scale at all, any quantitative conclusion on viscosity, however, should better rely on FEM calculations, including all just mentioned properties. This viscosity prediction has then to be compared with measured viscosity data utilizing the excellent literature background for various methods like penetration [12], [13], rotational [14], parallel plate [15], or sinter-related viscometry [16]. Such a FEM-approach could also be extended to other geometries and time scales useable for optical in-line viscosity measurements as e.g. reported for fused silica glass [17] or as an alternate to mechanically in-line methods as e.g. reported for polymer glass melts [18], [19], [20].

Another application limit of the proposed method could be related to the melting temperature. Although the method was tested for several sodium-alumino-borosilicate glasses in as much as the reflected image of the camera observation tube and its vibration after applying a

mechanical impulse could be clearly seen, increased temperatures could cause a strongly increased radiation background. This would rise the difficulties to reach the required grey value differences. In this case, however, the use of an additional light source as e.g. a laser light beam would allow to overcome this problem.

7. Summary

This paper presents a simple real-time method for evaluating the castability of glass melts. The method is based on analysing successive top-view images of the melt inside the furnace after being subjected to a small mechanical impulse. In this way, the melt surface in the crucible is excited to oscillate below a certain limit of viscosity. In the present case, the image contrast differences during oscillation were intensified by the shifted reflection image of the observation tube in the inner furnace roof.

Although the method can also be applied to other laboratory furnaces, it offers particular advantages for high-throughput glass melting systems. As it is based on the continuous camera observation of the melt and the image analysis has been kept as simple as possible, it provides a real-time check of the castability of the melt. This check can return a system query parameter for the interruption of improperly programmed casting steps as an emergency stop. In this way, the probability of system failure is reduced and the capacity of the system is increased due to the possible reduction of safety margins in casting temperature and time. As the method enables the detection of low viscosity, it ensures better casting reproducibility and helps to reduce melt fracture remaining in the crucible after casting. Finally, as the mechanical impulse that causes the vibration of the melt surface can be applied inside the furnace, no process step to interrupt the melt or special technical equipment is required. The required camera and observation tube can also be used for other purposes such as batch melting or foam control and can become part of an integrated process monitoring.

Data availability statement

Data will be made available on request.

Author contributions

H. Bornhöft performed the experiments with glass melting, designed the concept of data analysis and wrote the manuscript with support from S. Gogula. S. Gogula designed the computational framework, wrote the software and analysed the data. R. Müller wrote the final version of the manuscript. J. Deubener supervised the project and contributed to the final version of the manuscript. L. Wondraczek, M. Sierka, A. Diegeler, R. Müller, and J. Deubener were involved in funding acquisition.

Competing interests

The authors declare that they have no competing interests.

Acknowledgement

The present work was part of the joint project GlasDigital [4], which in turn was embedded in the *MaterialDigital* initiative of the Federal Ministry of Education and Research (BMBF). The authors would like to thank Dr. S. Pieper (VDI) for his encouraging unbureaucratic project supervision and the GlasDigital project team for the continuous openminded, fair, and inspiring

cooperation. Special thanks to T. Waurischk, C. Meyer and S. Reinsch, Bundesanstalt für Materialforschung und -prüfung (BAM), Berlin, for providing glass batches and helpful discussions.

Funding

The authors would like to thank the BMBF for financial support (# 13XP5122B).

List of variables

x,y	Image pixel coordination ($x, y = 1-240$ for the accessible image section, 1-120 and 121-240 for image quadrants)
t	image acquisition time
Δt	time difference between consecutive images ($t \approx 0.33$ s at 30 fps)
$RGB(x,y)_t$	8-bit colour image ($R, G, B = 0-255$) taken at t
$I(x,y)_t$	8-bit grey value image ($I = 0-255$) calculated from $RGB(x,y)_t$
$I_{eq}(x,y)_t$	8-bit grey value image with a corrected grey value distribution calculated from $I(x,y)_t$
$\Delta I_{eq}(x,y)_t$	8-bit absolute grey value difference between consecutive images $I_{eq}(x,y)_t$ and $\Delta I_{eq}(x,y)_{t+\Delta t}$
$\Delta I_{bw}(x,y)_t$	2-bit black and white image indicating $\Delta I_{eq}(x,y)_t > 30$ by white pixels ($I_{bw} = 255$)
D_t	Number of white pixels per image quadrant of $\Delta I_{bw}(x,y)_t$ ($D_t = 0-14400$)
$\langle \Delta D \rangle$	Average of $\Delta D(t)$
$CV_D(T)$	Coefficient of variation of D_t

References

- [1] E.D. Zanotto, F.A.B. Coutinho, "How many non-crystalline solids can be made from all the elements of the periodic table?", J Non-Crystal. Solids, vol. 347 no.1-3, 2004, pp. 285-288, ISSN 0022-3093.
- [2] W. Höland, G.H. Beall, "Applications of Glass-Ceramics" in Glass-Ceramic Technol., 2nd edition, Westerville, OH, The Ameri. Ceram. Soc., 2002, ch. 4.1 Technical Appl., pp. 252-353. DOI 10.1002/9781118265987.
- [3] A. K. Varshneya, "Introduction" in "Fundamentals of Inorganic Glasses", 1st edition., San Diego, CA, Academic Press, 1994, ch.1, pp. 1-11, ISBN-13: 978-0127149707.
- [4] Datengetriebener Workflow für die beschleunigte Entwicklung von Glas, Contact: T. Waurischk, *<https://materialdigital.de/project/4>
- [5] R. C. Gonzalez, R. E. Woods, "Digital Image Processing", 4th edition. Pearson, New York, NY 10013, John Wiley & Sons, 2018. ISBN 978-0-13-335672-4, pp. 185.
- [6] A. K. Jain, Fundamentals of Digital Image Processing. Englewood Cliffs, NJ: Prentice Hall, 1989, pp. 569, ISBN: 0133325784, 9780133325782.
- [7] OpenCV – Open Computer Vision Library, Developer Intel, Willow Garage: *<https://opencv.org/>
- [8] Recommendation ITU-R (03/11): "Studio encoding parameters of digital television for standard 4:3 and wide-screen 16:9 aspect ratios, https://www.itu.int/dms_pubrec/itu-r/rec/bt/R-REC-BT.601-7-201103-I!!PDF-E.pdf
- [9] OpenCV Histogram Equalization and Adaptive Histogram Equalization (CLAHE), A. Rosebrock, February 1, 2021 *<https://pyimagesearch.com/2021/02/01/opencv-histogram-equalization-and-adaptive-histogram-equalization-clahe/>
- [10] OpenCV-Python Tutorials / Image Processing in OpenCV / Histograms in OpenCV in OpenCV – Open Computer Vision Library, Developer Intel, Willow Garage: *https://docs.opencv.org/4.x/d5/daf/tutorial_py_histogram_equalization.html
- [11] Viskosität, 237 Authors, *<https://de.wikipedia.org/wiki/Viskosit%C3%A4t> * last date accessed:10.6.2024
- [12] A. Dietzel, R. Brückner, "Ein Fixpunkt der Zähigkeit im Verarbeitungsbereich der Gläser. Schnellbestimmung des Viskositäts-Temperatur-Verlaufs", Glastechn. Ber., vol. 30, no. 3, 1957, p.73-78,
- [13] R. Brückner, G. Demharter, „Systematische Untersuchungen über die Anwendbarkeit von Penetrationsviskosimetern“, Glastechn. Ber., vol. 48, no. 1, 1975, p.12-78.

- [14] G. Meerlender, „A Rotational Method for Measuring the Viscosity of Glass in the Range between Strain Point and Melting Temperatures”, Proc. 4th Intern. Congr. On Rheology, Providence 1963, Part 3, John Wiley & Sons, New York 1965
- [15] A. N. Gent, “Theory of the parallel plate viscometer”, Brit. Journal Applied Phys., vol. 11, 1960, pp. 85-87
- [16] M. J. Pascual, A. Duran, M. O. Prado, “A new method for determining fixed viscosity points of glass”, Phys. Chem. Glasses, vol. 45, 2005, no. 5, pp. 512-520
- [17] Paek, U. C., Schroeder, C. M., & Kurkjian, C. R. (1988), “Determination of the viscosity of high silica glasses during fibre drawing”, Glass technology, vol. 29, no. 6, pp. 263-266.
- [18] T. J. Coogan, D. O. Kazmer, “In-line rheological monitoring of fused deposition modeling.”, J. Rheol., vol. 63, no. 1, 2019, pp. 141–155, <https://doi.org/10.1122/1.5054648>
- [19] H. Bissig, O., Bükler, K., Stolt, E., Graham, L., Wales, A., Furtado, J. C. Lötters, “First comparison of inline measurements of dynamic viscosity”, in proc. 19th International Flow Measurement Conference 2022, FLOMEKO 2022. International Measurement Confederation (IMEKO).
- [20] V.S.K. Prasad, K. Balasubramaniam, E. Kannan, K.L. Geisinger, „Viscosity measurements of melts at high temperatures using ultrasonic guided waves”, J of Mat. Processing Technol. Vol. 207, no. 1–3, 2008, pp- 315-320, ISSN 0924-0136, <https://doi.org/10.1016/j.jmatprotec.2008.06.049>.